

Model Order Reduction of Combustion Processes with Complex Front Dynamics

Philipp Krah^{1,2}, Mario Sroka¹, and Julius Reiss¹

¹Technische Universität Berlin, Institut für Strömungsmechanik und Technische Akustik (TUB), Müller-Breslau-Straße 15, 10623 Berlin

²Institut für Mathematik, Technische Universität Berlin, Straße des 17. Juni 136, 10623 Berlin

Abstract. In this work we present a data driven method, used to improve mode-based model order reduction of transport fields with sharp fronts. We assume that the original flow field $q(\mathbf{x}, t) = f(\phi(\mathbf{x}, t))$ can be reconstructed by a front shape function f and a level set function ϕ . The level set function is used to generate a local coordinate, which parametrizes the distance to the front. In this way, we are able to embed the local 1D description of the front for complex 2D front dynamics with merging or splitting fronts, while seeking a low rank description of ϕ . Here, the freedom of choosing ϕ far away from the front can be used to find a low rank description of ϕ which accelerates the convergence of $\|q - f(\phi_n)\|$, when truncating ϕ after the n th mode. We demonstrate the ability of this new ansatz for a 2D propagating flame with a moving front.

1 Introduction

Nowadays combustion systems are studied by simulating the reactive Navier Stokes equations with billions of degrees of freedom. The simulations are numerically expensive, because computational resources scale with the number of degrees of freedom. Therefore, model order reduction (MOR) techniques are desired to reduce the number of relevant parameters, which describe the system. Unfortunately, classical MOR techniques fail for these systems. We aim for an improvement in this report.

Our method follows a data driven approach, where a set of N snapshots, $\{q(\mathbf{x}, t_i)\}_{i=1,\dots,N}$, gathered during a numerical simulation, is used to generate a reduced order model (ROM). Here, most ROMs rely on separation of variables:

$$q(\mathbf{x}, t) \approx \sum_{i=1}^n a_i(t) \psi_i(\mathbf{x}) \quad (1)$$

in which the initial high fidelity field $q(\mathbf{x}, t)$ is represented by a set of basis functions ψ_i and their amplitudes a_i . Based on eq. (1), Petrov Galerkin and Galerkin methods (see for a review [1]) project the original dynamics on a n -dimensional subspace spanned by the basis ψ_i . However, the approximation error of the produced ROM crucially depends on the error made in eq. (1). Unfortunately, in combustion systems transport dominated phenomena like moving flame kernels with sharp gradients or

traveling shock waves critically slow down the convergence of eq. (1). For instance, this was numerically investigated by [2] for reactive flows and is theoretically quantified with help of the Kolmogorov n -width [3, 4].

In order to handle transport dominated fields with sharp fronts, we propose a nonlinear mapping of the solution manifold:

$$q(\mathbf{x}, t) = f(\phi) \quad \text{s. t. } \phi(\mathbf{x}, t) = \sum_{i=1}^n \tilde{a}_i(t) \tilde{\psi}_i(\mathbf{x}). \quad (2)$$

Here, the function $f : \mathbb{R} \rightarrow \mathbb{R}$ is simply the wave profile and ϕ describes the shift of the wave profile in time.

This approach shares similar features as [5, 6, 8, 11], but overcomes some of the problems associated with these methods. Namely, [5, 11] depends on the choice of the shifts or their a priori knowledge and becomes cumbersome if the topology of the moving object changes. The latter is also the main drawback of [8]. Furthermore, [5, 8] are mainly applied in one spatial dimension. Although [6] does not suffer from the aforementioned drawbacks, it lacks physical interpretation and provides little insight of the underlying structure.

The report is organized as follows: In the first two sections we introduce the basic idea for 1D and 2D advective systems and explain the benefits of our concept. One possible realization is provided in section 4, which is then applied to a real life application in combustion – the reduction of burning hydrogen with complex front dynamics including topological changes (section 5). Finally, we come back to [5–8] by comparing the concept (section 6).

2 Basic Idea: 1D example - advective transport

To motivate the proposed method we first consider a one dimensional problem. A field $q(x, t)$ defined on $\mathcal{V} = [0, L] \times [0, T]$, with $L, T > 0$ is given by

$$q(x, t) = f(\phi(x, t)), \quad (3)$$

where f is a non-linear function and the auxiliary field $\phi(x, t) = x - \Delta(t)$. This describes an advective transport with trajectory path $\Delta(t) : [0, T] \rightarrow \mathbb{R}$, in the most simple example $\Delta(t) = ct$ with transport speed c . The function f is assumed to have a large gradient near $\phi = 0$. In the examples we use

$$f_\lambda(\phi) = (\tanh(\phi/\lambda) + 1)/2, \quad (4)$$

where $\lambda > 0$ adjusts the front width. Snapshots of the functions q and ϕ are plotted for increasing time t in fig. 1, left. The corresponding snapshot matrices X^ϕ, X^q are defined as usual, $X_{i,j}^\alpha = \alpha(x_i, t_j)$. A common approach to find a small representation of X^α is the truncated singular value decomposition (SVD)

$$X_n^\alpha = \sum_{k=1}^n \sigma_k \mathbf{u}_k \mathbf{v}_k^\top \hat{=} \sum_{k=1}^n a_k(t) \psi_k(\mathbf{x}), \quad (5)$$

which approximates X^α in the sense that the residuum $\mathcal{R} = X^\alpha - X_n^\alpha$ is minimized. We call the orthonormal basis $\{\psi_k(x_i) = (\mathbf{v}_k)_i\}_{i=1,\dots,n}$ spatial modes and $\{a_k(t_i) = (\sigma_k \mathbf{u}_k)_i\}_{i=1,\dots,n}$ temporal coefficients. As known from the Eckart Young Theorem [9], the approximation error $\|X^\alpha - X_n^\alpha\|_2^2$ ¹ is given by the

¹Note that for simplicity we will also use $\|\alpha - \tilde{\alpha}\|_2$ for scalar functions $\alpha : \mathcal{V} \rightarrow \mathbb{R}$. which we actually calculate as $\|X^\alpha - X^{\tilde{\alpha}}\|_2$.

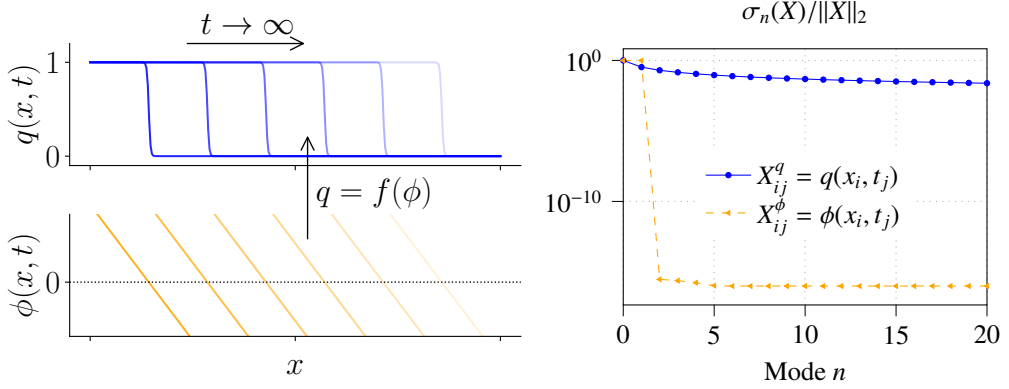


Figure 1. Transported quantities q and ϕ and singular values of the associated snapshotmatrix X^q and X^ϕ . Both functions share the same transport, since $q = f(\phi)$. However the transport of the sharp front is not well presented by a linear ansatz, eq. (5), and therefore the singular values decay substantially slower as for the smooth field ϕ .

singular value σ_{n+1} , when truncating after the n th spatial mode. The acceptable residuum is typically determined by the target application. A small number n is desired in model order reduction as it governs the numerical cost of the reduced model.

In fig. 1, right we see the decay of the truncated singular value decomposition eq. (5) of X^q and X^ϕ is fundamentally different, even though q is created from ϕ and both share the same advective transport. The failure of the SVD or POD to represent sharp transports is well known [3]. In contrast to our example, ϕ can be represented by a linear combination of two functions $\{x, 1\}$. Here, transport of the field ϕ is simply an amplitude change of the constant function. This fact is not new and exploited by ([5, 10]).

With this ansatz we aim for a generalization of the method to higher spatial dimensions, by representing the movement of a front by an auxiliary field ϕ which is of low rank and a nonlinear mapping f to recover the original field. Thereby a locally one dimensional transport is implied. However, we abstain from a global transport map between snapshots, as this obstructs the application for topology changes.

3 2D Example - Moving Disc

The setting is now illustrated for a two dimensional problem of a disc with radius $R = 0.15L$, moving in a circle in a $[0, L]^2$ domain. The translation of the disc is parametrized by:

$$q(\mathbf{x}, t) = f(\phi(\mathbf{x}, t)) \quad \text{and} \quad \phi(\mathbf{x}, t) = \|\mathbf{x} - \mathbf{x}_0(t)\|_2 - R \quad (6)$$

$$\text{where } \mathbf{x}_0(t) = L \begin{pmatrix} 0.5 + 1/4 \cos(2\pi t) \\ 0.5 + 1/4 \sin(2\pi t) \end{pmatrix}, \quad (7)$$

and f is again the step function defined in eq. (4). We sample 60 snapshots in a time interval $[0, 1]$. ϕ is the signed distance function shown in the left of fig. 2, which shall mimic the ϕ of the one dimensional example close to $\phi \approx 0$.

The original field q is again reconstructed applying the SVD to ϕ from which the approximation $\tilde{q} = f(\phi_n)$ is obtained. Figure 2 shows the comparison between the reconstruction using $f(\phi_n)$ and

the naive POD approach using q_n for snapshot $t = 1/4$ with $n = 10$ modes. The results show not only a reduction in the overall error but also that the basic structure of the moving disc is recovered. The latter is already the case for a small number of modes. While the example shows that the concept

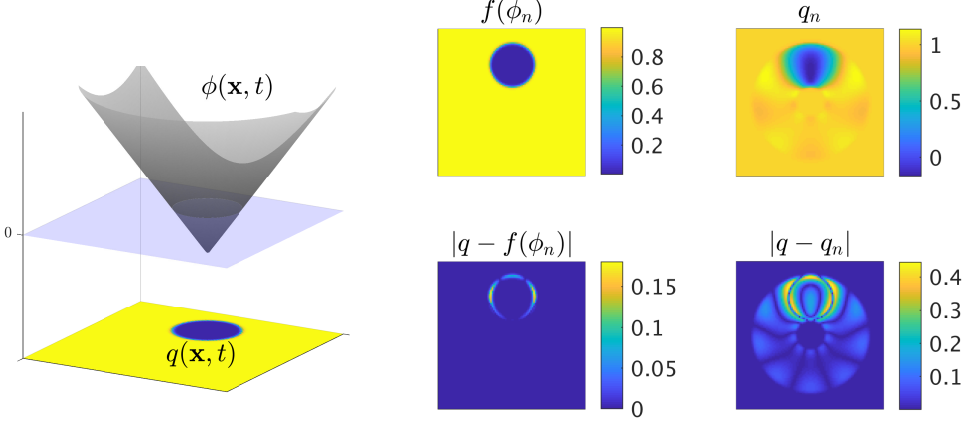


Figure 2. Left: visualization of the signed distance function. Right: Reconstruction of q with $n = 10$ modes.

works well for 2D problems, we show that the choice of ϕ has a strong effect on the possible reduction. By replacing ϕ with a paraboloid $\varphi(\mathbf{x}, t) = \frac{1}{2R}(\|\mathbf{x} - \mathbf{x}_0(t)\|_2^2 - R^2)$ in eq. (6), it is possible to obtain a much smaller error with less spatial modes. A one dimensional profile of the two functions ϕ, φ is plotted in the left of fig. 3. Note that ϕ and φ have the same zero-level and their gradients are identical at the zero-level for all times t . Therefore $f(\varphi) \approx q = f(\phi)$ is a good approximation for small widths λ . In contrast to ϕ , the total error $\|q - f(\varphi_n)\|_2$ is reduced to its minimum with only three modes, because φ can be represented by $\{x^2 + y^2 + R^2, x, y\}$. This is shown in the second and third column of fig. 3. From the ansatz $q \approx f(\varphi)$ we can deduce two different errors contributing to the total error:

$$\|q - f(\varphi_n)\| \leq \underbrace{\|q - f(\varphi)\|}_{=\Delta f} + \|f'(\varphi)\mathcal{R}\| + \mathcal{O}(\|\mathcal{R}^2\|). \quad (8)$$

The truncation error of the SVD is $\mathcal{R} = \varphi - \varphi_n$ and the approximation error of the data is Δf . Consequently, for vanishing approximation error, the truncation error $\|f'(\varphi)\mathcal{R}\| \leq \|f'(\varphi)\| \sigma_{n+1}$ bounds the total error in the two norm. Therefore, the total error scales with the decaying singular values of ϕ . This behaviour can be seen in fig. 3. While for ϕ the relative truncation error aligns with the total error (middle), the error of φ in the right plot is dominated by the approximation error $\Delta f \approx 10^{-3}$.

From this example, we see that the ansatz is a good candidate for a low rank optimization of φ . In contrast to areas where $f'(\varphi) \neq 0$ and the field φ has to mimic a signed distance to the front, it can be chosen to minimize the truncation error far away from the zero level where $f'(\phi) = 0$. Additionally, in an optimization procedure one could relax the assumption of constant front width by imposing appropriate conditions on the slope of φ close to the zero level. However this does not lie within the scope of this work.

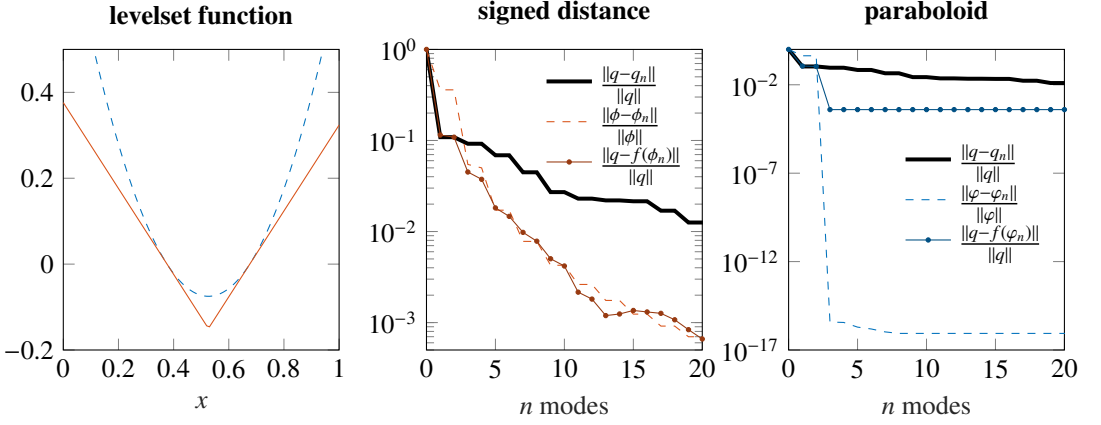


Figure 3. Left: Graphical visualization of the smoothed signed distance function ϕ defined in eq. (6) and the paraboloid $\varphi(\mathbf{x}, t) = \frac{1}{2R}(\|\mathbf{x} - \mathbf{x}_0(t)\|_2^2 - R^2)$ Left: A slice of ϕ and φ at $t = 0$ and $\mathbf{x} = (x, y_0)$, $x \in [0, L]$. Comparison of the different truncation errors for the signed distance (center) and paraboloid (right).

4 Front Transport Reconstruction (FTR)

Now, we proceed to extend the idea to numerical data. Here, only the field q is known and the auxiliary field ϕ and the front shape function f need to be determined. For this, we assume that the front location can be calculated using threshold search of the relevant variables.

As proof of our concept, we compute ϕ as a two dimensional signed distance function, because it is easy to compute and can be directly interpreted as a local 1D coordinate system. This is a special choice for ϕ which is likely to be sub-optimal as was shown in the previous section. The zero-level curve C_0 of ϕ is determined by a threshold search with threshold q_{C_0} . The discrete contour line C_0 was sampled at points where q had the value q_{C_0} on any vertical or horizontal gridline of our computational mesh. A linear interpolation of q between the grid points is used to determine the crossing. The distance $d_{C_0}(\mathbf{x})$ is calculated as the minimal distance to all sections of this curve, assumed to be linear between two points. The sign of ϕ is negative if $q(\mathbf{x}) < q_{C_0}$, and positive otherwise. With the described procedure we determine the signed distance function $\phi(\mathbf{x}, t_i)$ for every $t_i = i\Delta t$, $i = 1, \dots, N$.

At this point a value of ϕ and q is available at every grid point from which the front shape function f is to be determined such that $q = f(\phi)$. This is complicated by the fact that such relation is approximate and only discrete values are available. From the computed signed distance function we choose all grid points $\hat{\phi}_l = \phi(x_{i_l}, y_{j_l}, t_{i_l})$ with $|\hat{\phi}_l| \leq \Delta\phi$ on vertical, horizontal or diagonal lines which cross C_0 as support of the samples $\hat{q}_l = q(x_{i_l}, y_{j_l}, t_{i_l})$. The sample vectors $(\hat{\phi}_l, \hat{q}_l)$ are then interpolated on a predefined support set ϕ_1, \dots, ϕ_M which is used to find the corresponding interpolated values f_1, \dots, f_M minimizing the difference between \hat{q}_l and $f(\hat{\phi}_l)$.

5 2D Example - Application to Combustion

In this section we show that the described procedure is capable of reconstructing flow dynamics with inherent two dimensional transport including changing typology, which is difficult for methods building on a mapping between snapshots to remove transports.

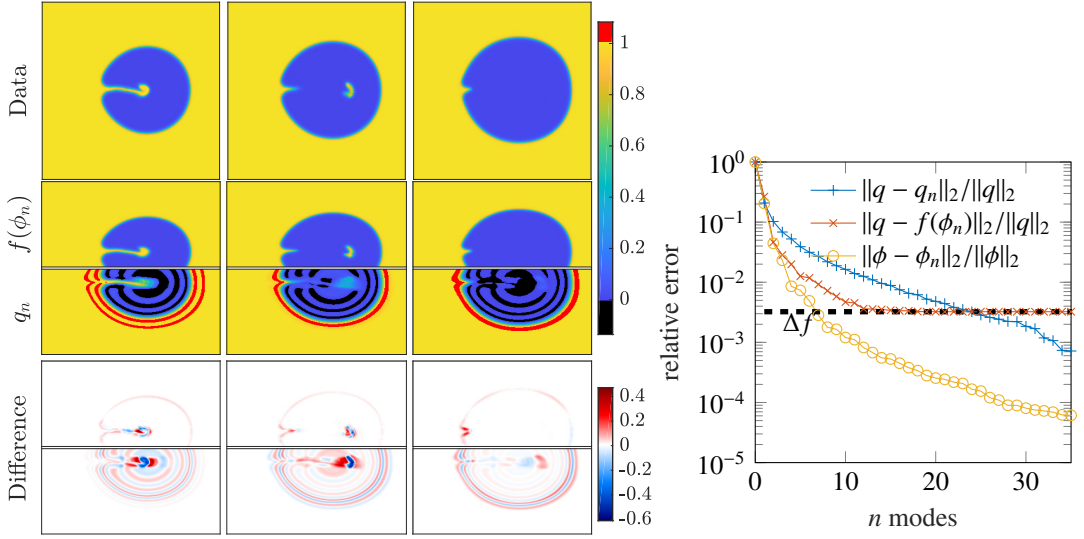


Figure 4. Comparison of q_n (POD) and $f(\phi_n)$ (levelset method). Left: Direct comparison of the snapshots $t/\Delta t = 21, 26, 31$ with q plotted in the first row, the approximations $f(\phi_n)$, q_n in the second row and the difference between the data and its approximation in the last row. Please note that the images in the lower rows contain only the fractions of the full snapshot that are relevant for our comparison. Right: Relative error in the two norm.

The configuration of a flame kernel interacting with a vortex pair mimics turbulence flame interaction. Our data set consists of 40 snapshots derived from a 2D simulation of the reactive Navier Stokes equations. For our purpose we restrict the reconstruction on the normalized mass fraction of hydrogen Y_{H_2} . The simulation was tuned such that a vortex pair moves towards burning H_2 and mixes unburned ($Y_{H_2} = 1$) with burned gas ($Y_{H_2} = 0$), such that a small bubble of unburned gas detaches into the burned area. The time evolution is visualized for some selected snapshots in the left of fig. 4. As seen from fig. 4, the Y_{H_2} snapshots contain a very interesting structure, in which the front changes along its contour line and even the topology of the line changes – splitting from one curve at $t/\Delta t = 24$ into two curves $t/\Delta t = 29$ and then back to a single curve at $t/\Delta t = 34$.

Applying the described procedure with a threshold of $q_{C_0} = 0.14$, we achieve promising results when comparing our method with a POD approximation in fig. 4 using 10 modes. For this specific data the threshold q_{C_0} was chosen to be rather small, in order to resolve the tail of the incoming bubble. The overall relative approximation error is decreased by a factor of three. More important, our approximation preserves the physical structure of the data. The POD does not respect the allowed physical range of $0 \leq Y_{H_2} \leq 1$ and shows staircasing, i.e. replaces a front by several fractional fronts. No sensible physical description can be expected from this structure. The new method, in contrast, has well defined fronts and respects the physical range, since f is by construction restricted to the range of the input data q .

6 Discussion and Conclusion

We presented a concept for modal decomposition of transported fronts. It builds on representing the original field q by an auxiliary field ϕ and a non-linear function f in such a way that the ϕ has a better low rank description than q . In a numerical example, ϕ was taken as a signed distance function with

the front as zero level and f describing the front shape. It is evident, that this choice is in general not optimal, since moving kinks in ϕ yield a slow decay of singular values.

This approach can be interpreted as embedding a local one dimensional coordinate into a multi-dimensional domain, orthogonal to the front. A transport in this direction is simply an additive term for ϕ . The time dependent shift to compensate a transport in one dimension is a special case of this approach. This induces a transport map, similar to [5, 10], with the important difference that there is a local but no global one to one mapping, by which topology changes are permitted. A different perspective is the comparison with neural networks. This linear combination to construct a low rank representation ϕ with the application of a non linear function can be seen as a one layer network with a special activation function f . A recent work uses level sets to handle geometry changes in which shares some technical aspects with the current work [11].

For full practical applicability, improvements are needed but near at hand. To improve the approximation error f and ϕ should be minimized based on eq. (8) and a more general ansatz should be used to allow a changing front shape.

Acknowledgments

This work is supported by the Deutsche Forschungsgemeinschaft (DFG, German Research Foundation) - 384950143/ GRK2433 and Project 200291049 - SFB 1029

References

- [1] C.W. Rowley, T. Colonius, R.M. Murray, *Physica D: Nonlinear Phenomena* **189**, 115 (2004)
- [2] C. Huang, K. Duraisamy, C. Merkle, *Challenges in Reduced Order Modeling of Reacting Flows*, in *2018 Joint Propulsion Conference* (2018), p. 4675
- [3] M. Ohlberger, S. Rave, arXiv preprint arXiv:1511.02021 (2015)
- [4] C. Greif, K. Urban, *Applied Mathematics Letters* **96**, 216 (2019)
- [5] J. Reiss, P. Schulze, J. Sesterhenn, V. Mehrmann, *SIAM Journal on Scientific Computing* **40**, A1322 (2018)
- [6] K. Lee, K.T. Carlberg, *Journal of Computational Physics* p. 108973 (2019)
- [7] G. Welper, *SIAM Journal on Scientific Computing* **39**, A1225 (2017)
- [8] D. Rim, S. Moe, R.J. LeVeque, *SIAM/ASA Journal on Uncertainty Quantification* **6**, 118 (2018)
- [9] C. Eckart, G. Young, *Psychometrika* **1**, 211 (1936)
- [10] D. Rim, *SIAM Journal on Scientific Computing* **40**, A4184–A4207 (2018)
- [11] E.N. Karatzas, F. Ballarin, G. Rozza, arXiv preprint arXiv:1901.03846 (2019)